

---

**Innovations Deserving  
Exploratory Analysis Programs**

***Rail Safety IDEA Program***

---

## **Ballast Real-time Information System**

Final Report for  
Rail Safety IDEA Project 30

Prepared by:  
Hai Huang  
Pennsylvania State University

***April 2019***

---

 TRANSPORTATION RESEARCH BOARD  
*The National Academies of*  
SCIENCES • ENGINEERING • MEDICINE



**Project Title:**

Ballast Real-time Information System

IDEA Program Final Report

**Reporting Period:**

1/1/2017 – 4/15/2019

**Contract Number:**

IDEA Rail Safety

IDEA Program  
Transportation Research Board  
National Research Council

Hai Huang  
Pennsylvania State University

4/15/2019

**TABLE OF CONTENTS**

Executive Summary..... 1

IDEA Product ..... 3

    I. Ballast Real-time Information System (BRIS) for ballast particle movements detection..... 3

    II. “SmartRocks” network for ballast fouling detection..... 3

    III. SMART Computing algorithm..... 3

Concept and Innovation..... 4

Investigation..... 5

    I. System, Hardware and Software manufacturing for BRIS including redesign and manufacturing of SmartRocks ..... 5

    II. Laboratory testing of the “SmartRock” network for reliability and durability..... 6

    III. Field application and system demonstration..... 8

    IV. Laboratory development of the “Critical” Ballast Particle Movement Patterns..... 11

    V. Connect “SmartRock” network with cloud DEM computing to predict ballast performance..... 20

Conclusions..... 30

**RAIL SAFETY IDEA PROGRAM  
COMMITTEE**

**CHAIR**

CONRAD RUPPERT, JR.  
*Railway Engineering Educator  
& Consultant*

**MEMBERS**

TOM BARTLETT  
*Transportation Product Sales Company*  
MELVIN CLARK  
*LTK Engineering Services*  
MICHAEL FRANKE  
*Retired Amtrak*  
BRAD KERCHOF  
*Norfolk Southern Railway*  
MARTITA MULLEN  
*Canadian National Railway*  
STEPHEN M. POPKIN  
*Volpe National Transportation Systems  
Center*

**FRA LIAISON**

TAREK OMAR  
*Federal Railroad Administration*

**TRB LIAISON**

SCOTT BABCOCK  
*Transportation Research Board*

**IDEA PROGRAMS STAFF**

GWEN CHISHOLM-SMITH, *Manager, Transit  
Cooperative Research Program*  
VELVET BASEMERA-FITZPATRICK, *Senior  
Program Officer*  
DEMISHA WILLIAMS, *Senior Program Assistant*

**EXPERT REVIEW**

**PANEL SAFETY IDEA**

**PROJECT 34**

William Dombrow, *BNSF*  
Dingqing Li, *Transportation Technology Center,  
Inc.*  
Joe Smak, *Amtrak*



## Executive Summary

Ballast is an important part of railroad infrastructure. It is used as a support base for bearing the load from the track, as well as facilitating drainage of water from the track. Hence, the ballast layer serves an important role in track performance. This IDEA project aims to develop and validate an integrated system – Ballast Real-time information System (BRIS) – of hardware (SmartRocks) and software (Smart Computing) components that can predict track substructure safety concerns due to aggregate movement.

“SmartRock”, a wireless embedded sensor, was manufactured to form connected communication network system which consists of multiple SmartRocks, a solar panel, antenna, remote monitoring device, Wi-Fi hotspot, and data acquisition (DAQ) box containing a storage battery, power inverter, and data acquisition system. The DAQ box works as a trackside host to communicate with the SmartRocks and enables them to start data collection and transmission. The host can then pass the SmartRock data to the cloud computing center using Wi-Fi. A user interface (software) that will allow engineers to customize SmartRock network parameters after installation, such as sampling frequency, sampling strategy, warning threshold, etc. has been developed (a Graphical User Interface is available upon request).

To make sure SmartRocks could reflect the actual granite ballast particle movements and test the communication quality and reliability, service life, and durability of the “SmartRock”, both a laboratory test and field installation have been conducted. Furthermore, during the field application, five “SmartRocks” were installed at the NS mainline (Class 4) near Bellwood, PA with two sites including one control site with clean ballast and one mud pumping site chosen. The results show SmartRocks are capable to record the different particle movements under different ballast conditions.

Laboratory experiments were also performed at Penn State with a ballast box with dimensions of 3.96 m (long)  $\times$  3.36 m (wide)  $\times$  1.22 m (high) and a loading system for simulating the moving train load. During the laboratory test, a series of ballast box tests were conducted to investigate the ballast particle movement pattern inside railway ballast under different ballast, loading, moisture, and shoulder confinement conditions. Eight wireless embedded devices - “SmartRocks” - were used in the laboratory tests in three different locations to study different ballast movement patterns under different conditions.

From the laboratory testing results, SmartRocks are confirmed to be capable of recording particle movements under different ballast, loading, and moisture conditions; and may serve as a potential monitoring tool to monitor the ballast behavior and performance; The magnitude of ballast particle movement depends on track conditions: a track with mud pumping is likely have greater ballast particle movement; The influence of moisture content on particle movements in the clean and fouled ballast is different. The intrusion of fine particles in fouled ballast affects the drainage capacity of the ballast. The particle movements are much more sensitive to moisture content for the fouled ballast than the clean ballast.

Finally, connections between “SmartRock” network has been set up and a computing scheme that is based on real-time data fusion between a sensing mechanism and real time (SMART) computing was developed, implemented and validated. Laboratory large-scale triaxial tests on ballast specimens were conducted and the results were compared to traditional DEM-only and SMART computing simulations. Results indicate that the SMART computing, if implemented with appropriate physical models, can be used to simulate the large-scale shearing tests with high fidelity and accuracy.

The specific accomplishments of this project were to:

- System, Hardware and Software manufacturing for BRIS including redesign and manufacturing of SmartRocks;
- Laboratory testing of the “SmartRock” network for reliability and durability;
- Field application and system demonstration;
- Laboratory development of the “Critical” Ballast Particle Movement Patterns;
- Connect “SmartRock” network with cloud DEM computing to predict ballast performance;

## **IDEA Product**

### **I. Ballast Real-time Information System (BRIS) for ballast particle movements detection**

“SmartRocks”, wireless embedded sensors, were manufactured to form BRIS. This system consisted of multiple SmartRocks, a solar panel, antenna, remote monitoring device, Wi-Fi hotspot, and data acquisition (DAQ) box containing a storage battery, power inverter, and data acquisition system. A user interface (software) that will allow engineers to customize SmartRock network parameters after installation, such as sampling frequency, sampling strategy, warning threshold, etc. has been developed (a Graphical User Interface is available upon request). BRIS system could be installed in the lab and field for measuring ballast particle movements under different ballast conditions.

### **II. “SmartRocks” network for ballast fouling detection**

A series of ballast box tests with a full-scale railway track structure has been conducted and approved that SmartRocks are capable of recording particle movements under different ballast, loading, and moisture conditions; and may serve as a potential monitoring tool to monitor the ballast behavior and performance.

### **III. SMART Computing algorithm**

SMART computing algorithm that can enhance DEM simulations using a wireless device - “SmartRock.” The SmartRock is capable of recording real-time particle translation and rotation if embedded in a granular assembly. The SMART computing is a Kalman-filter-based data fusion technique that can incorporate real-time SmartRock recordings into DEM simulations to improve the accuracy of the simulation. The SMART computing, if implemented with appropriate physical models, can be used to simulate the large-scale shearing tests with high fidelity and accuracy.

## **Concept and Innovation**

Ballast track performance and safety are largely dependent on ballast service conditions. Unfavorable ballast conditions (or “ballast defects”) will cause track geometry roughness and can contribute to increased rates of damage and deterioration to the rail, tie and fastening components. The Federal Railroad Administration (FRA) issued a safety advisory in 2015 to emphasize the importance of timely repairs of ballast defects and conditions on main track. Ballast defects, if untreated, will eventually lead to ballast failure. In-service ballast failure, which is defined as rapid deformation within only a few hundred load cycles, is a critical safety issue for railroad operations. Although ballast defects are often apparent through indications of poor geometry and structural degradation, maintenance and repair should be taken before the track displays noticeable deterioration in geometry. Further, advanced technologies are needed to predict the possibility of future ballast in-service failure so that timely warnings to the train/locomotive engineer can be issued.

The objective of this research is to develop and test an innovative “Ballast Real-time Information System (BRIS)” based on “SmartRock” technology that can detect “non-visual” (i.e. by track inspectors) ballast defects (usually early stage) and predict the possibility of future ballast in-service failure.

“SmartRock” is a wireless device developed by the Principal Investigator (PI) under the financial support from FRA-BAA. It can sense, record, and transmit its movement including: linear and rotational acceleration, velocity, and displacement in real time. It has user defined sizes and shapes that fit many civil engineering applications in the area of unbound particulate material. 3D printing technology was employed to generate the shape of the “SmartRock”. Details of the “SmartRock” can be found in Liu et al, 2015. The visualization algorithm comes with the product and is able to visualize not only the movement but also the exact shape of the “SmartRock” in real time. When “SmartRocks” are installed in the field, researchers at Penn State (or future railroad engineers) can easily see the movement on their computer screens simultaneously. “SmartRock” makes it possible for the first time to identify ballast defects/failure based on individual ballast particle movements.

Preliminary experiments indicate that if current ballast particle movement pattern can be successfully captured, it is possible to develop the links between ballast particle movement patterns and ballast defects/failure modes. It is also possible to predict future ballast particle movement pattern, for instance, under the next train loading. If the prediction came out to be unfavorable, i.e. ballast failure may happen, it is then expected that this information could be sent to the railroad for further investigation and decision making before the next train actually arrives. To that end, the “Ballast Real-time Information System (BRIS)” is proposed in this research.

## Investigation

There were three major goals of this project: Construction of a SmartRocks network system --- BRIS for monitoring ballast particle movements and recording, sensing the data to cloud computing; Laboratory and field applications for validating the network and studying the movement patterns; Incorporation of real-time SmartRock recordings into DEM simulations to improve the accuracy of the simulation. The specific goals of this project were solved by the following tasks:

### 1. System, Hardware and Software manufacturing for BRIS including redesign and manufacturing of SmartRocks

In this task, 14 “SmartRocks”, as shown in Figure 1, were manufactured to form connected communication networks system as shown in Figure 2. This network system consisted of multiple SmartRocks, a solar panel, antenna, remote monitoring device, Wi-Fi hotspot, and data acquisition (DAQ) box containing a storage battery, power inverter, and data acquisition system. The DAQ box works as a trackside host to communicate with the SmartRocks and enables them to start data collection and transmission. The host can then pass the SmartRock data to the cloud computing center using Wi-Fi. The SmartRocks were able to sleep between readings and reduce battery consumption via a power management system. The power management system let SmartRocks wake up at a desired time when the train was approaching the monitoring site; after the reading, the wireless connection was turned off, and the wakeup time was reset to when the next train was coming. This monitoring system was set up for remote operation.



Figure 1 SmartRocks during charging

In this project, each ballast cross section to be instrumented will be equipped with a track side “host” which can communicate with “SmartRocks” via Bluetooth. Two hosts were manufactured and tested in TTCI (Figure 2).

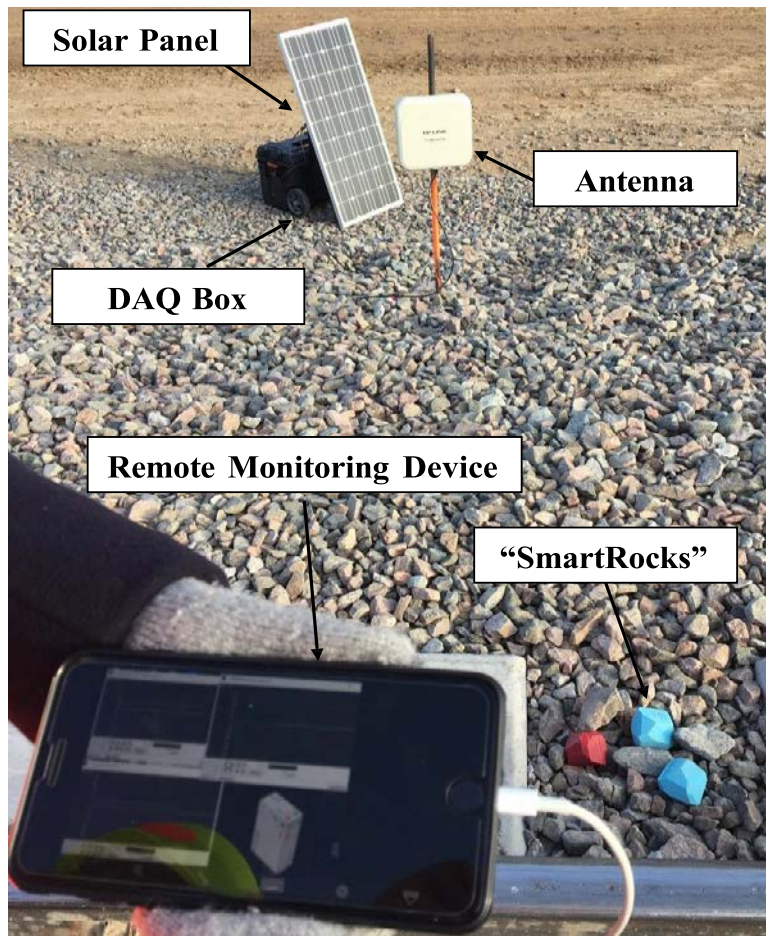


**Figure 2 Data Collection and remote-control Acquisition System**

A user interface (software) that will allow engineers to customize SmartRock network parameters after installation, such as sampling frequency, sampling strategy, warning threshold, etc. has been developed (a Graphical User Interface is available upon request).

## **2. Laboratory testing of the “SmartRock” network for reliability and durability**

To make sure SmartRocks will reflect the actual granite ballast particle movements, a SmartRock with granite rock shell was manufactured and tested to compare the recorded movements and interactions with those of the SmartRock with 3D printed shell (Figure 3). Also, communication quality and reliability, service life, and durability of the “SmartRock” network were tested in the Lab environment (Figure 4).



**Figure 3 A granite rock shell**

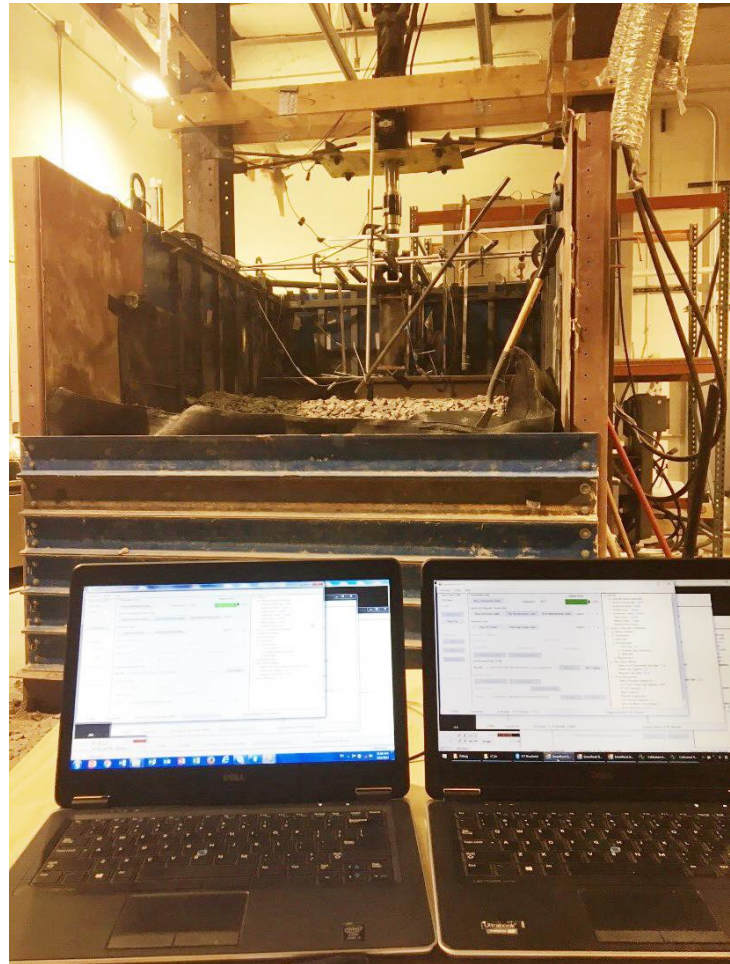


**Figure 4 Ballast box testing with SmartRocks installed**

### 3. Field application and system demonstration

The project team installed several “SmartRocks” in an NS Class 4 mainline track near Bellwood, PA. Two sites including one control site with clean ballast and one with mud pumping were chosen. These two sites were in close proximity on the same tangent track so that the train traffic was identical. Five “SmartRocks” were installed at each site, including underneath the tie as well as in the adjacent crib. An accelerometer was mounted on each tie so that the tie movement could be captured. Both freight and AMTRAK trains operated over the test site. Figure 5 shows pictures of the sites and the instrumentation. The upper left image shows the clean ballast section with a wireless accelerometer mounted on the tie. The upper right image shows the tie at the mud spot with the same type of accelerometer (different colors were used to differentiate these two sites). The lower left image shows the SmartRocks before installation and lower right image show the signal receiver for both accelerometers and the SmartRocks buried underneath those ties.



Figure 5 “SmartRock” installation at the NS mainline Bellwood, PA

Figure 6 compares the movement data reported by the SmartRocks in the cribs from both sites under a freight train. The Power Spectral Density (PSD) of the vertical accelerations were plotted in this case. PSD is not only a strong indication of the movement intensity, but also shows the strength of the variations (e.g., energy) as a function of frequency; in other words, it shows at which frequencies variations are strong and at which frequencies variations are weak. The procedures to compute PSD are shown as follow:

- a. Compute the Fourier transform of the data sequence  $X(n)$

$$X(n) \leftrightarrow X(f)$$

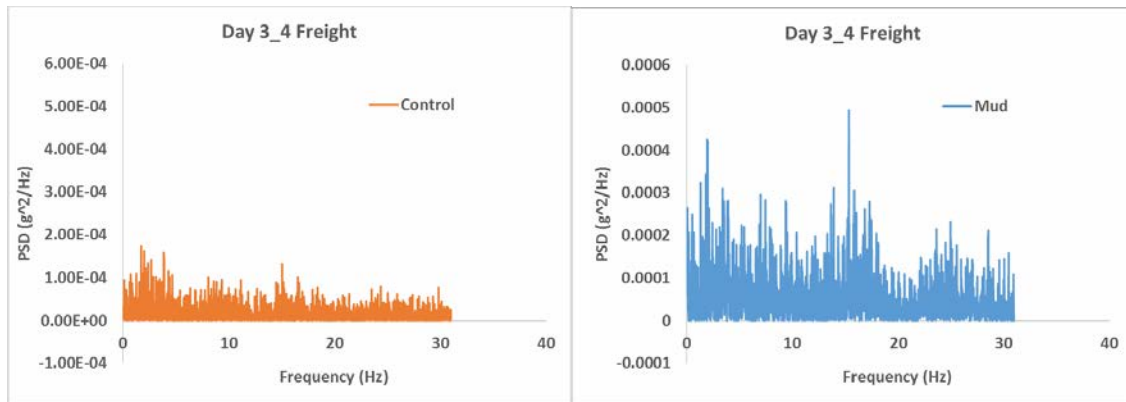
- b. Multiply  $X(f)$  by its conjugate to obtain the power spectral density  $S_{N_{xx}}(f)$

$$S_{N_{xx}}(f) = \frac{1}{N} |X(f)|^2$$

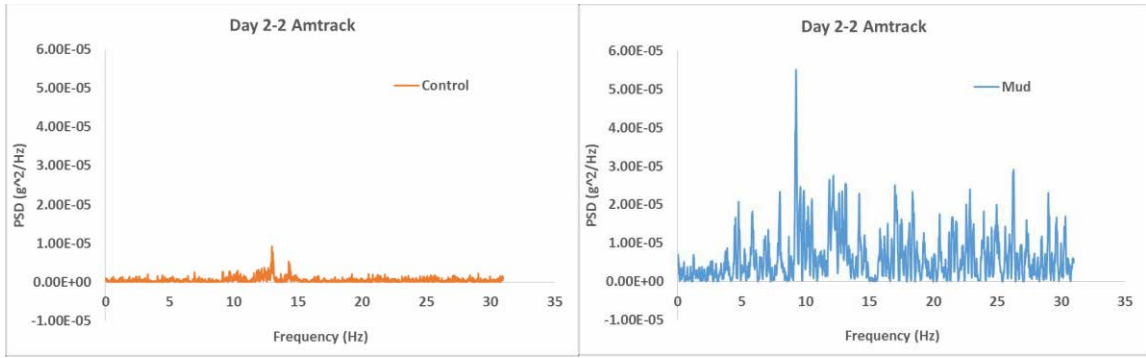
- c. Convolve  $S_{N_{xx}}(f)$  with an appropriate window function  $W(f)$

$$S_{W_{xx}}(f) = S_{N_{xx}}(f) * W(f)$$

The values of PSD were automatically computed using professional signal processing software SigView as an input of acceleration. Results in Figures 6 and 7 both show that the SmartRock in the crib area at the mud spot site experienced much more dramatic (about two times more) vertical vibration than the one at the control site which is likely due to a lack of particle-to-particle interlocking in the mud-spot site. In particular, Figure 7 shows the same plot for a passenger train (AMTRAK Pennsylvanian 42 service to Philadelphia) running at approximately 70 mph which is much faster than the freight train. It is surprising to see significantly greater particle movement in the mud spot site compared to the control site for a passenger train. This is likely due to the faster loading rate generated by a higher speed train and indicates possible high mud pressure generation in the crib area. The PSD response from the freight train, as shown in Figure 6, had a broader range of frequency components, which is due to the freight train consisting of cars with different lengths and wheel loads (a longer car results in a lower frequency, and a car with greater wheel loads results in greater power spectral density).

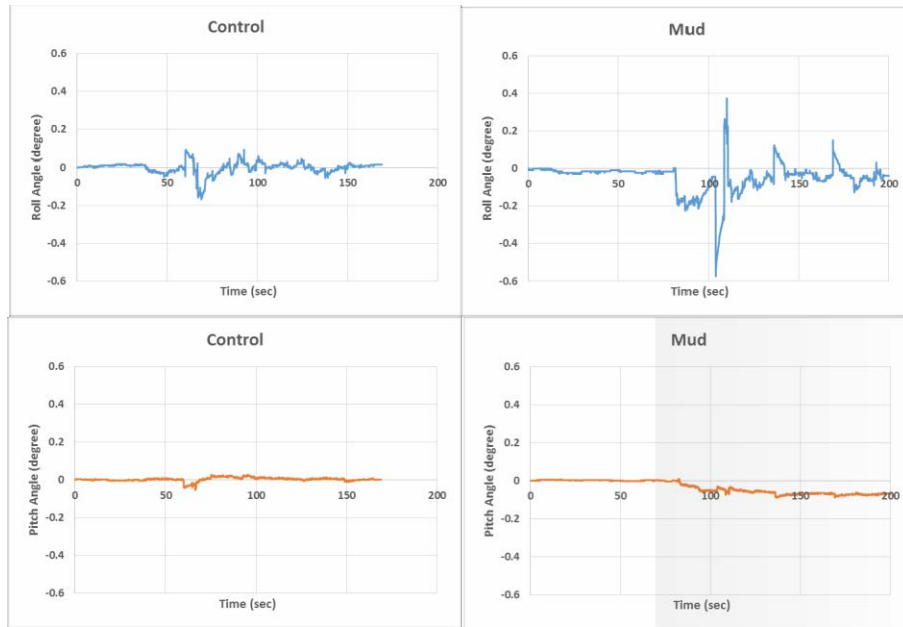


**Figure 6 Power Spectral Density of the vertical accelerations of the SmartRocks in the crib under freight train**



**Figure 7 Power Spectral Density of the vertical accelerations of the SmartRocks in the crib under passenger train**

Significant particle rotation is more likely to occur in the crib area due to lack of confinement, therefore, this location was used to study behavior of particle rotation in the clean and mud spot sites. Figure 8 compares the particle rotations in the crib area at the clean and mud spot sites. All three rotational angles (roll, pitch, and yaw) from both control and mud spot sites are plotted. It can be seen that while particles rotate in a similar manner and have similar magnitudes in pitch and yaw at both sites they do demonstrate a significant difference in terms of rolling, which is likely because of the slow operating speed towards track direction and heavy wheel load of the freight train having significant impact on the ballast particle movement.



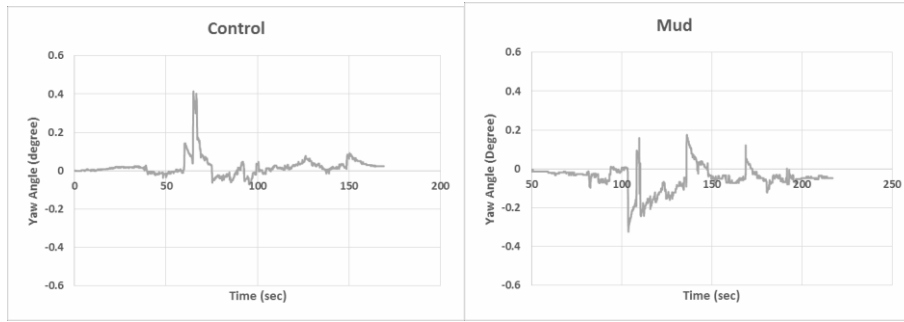


**Figure 8 Comparisons of particle rotation at both control and mud spot sites under freight train**

#### **4. Laboratory development of the “Critical” Ballast Particle Movement Patterns**

A clean ballast and a fouled ballast were used in this study. The clean ballast consisted of angular limestone aggregates, which conforms to the No. 3 gradation requirement of the American Railway Engineering and Maintenance-of-Way Association (AREMA) (see Figure 9). The fouled ballast was prepared by mixing the clean ballast with fine limestone particles (also Figure 9). The fouling index (FI) (Selig and Waters, 1994), which is the summation of the percentages passing the No. 4 sieve (4.75mm) and the No. 200 sieve (0.075mm), was used in this study to quantify and prepare the fouled ballast condition. In the calculation of FI, fines that passed the No. 200 sieve are accounted for twice due to the significance of fines in decreasing the drainage capacity. Based on the grain size distribution, the fouling index was 20.05%, which falls into the fouled ballast category based on the criteria developed by Selig and Waters (1994) and Indraratna et al. (2011).

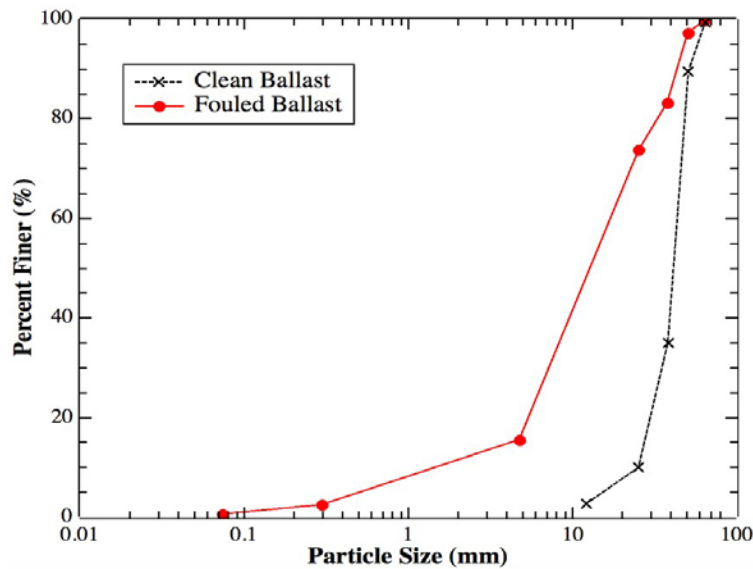


**Figure 9 Gradations of clean ballast and fouled ballast**

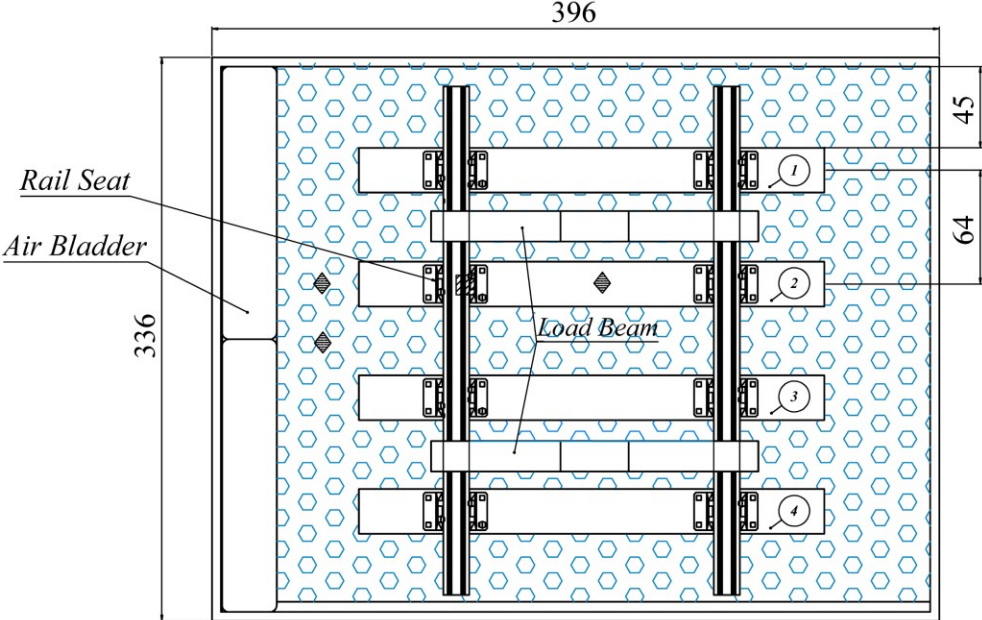
#### *Ballast Box and Instrumentation*

A ballast box with dimensions of 3.96 m (long) × 3.36 m (wide) × 1.22 m (high) and a loading system

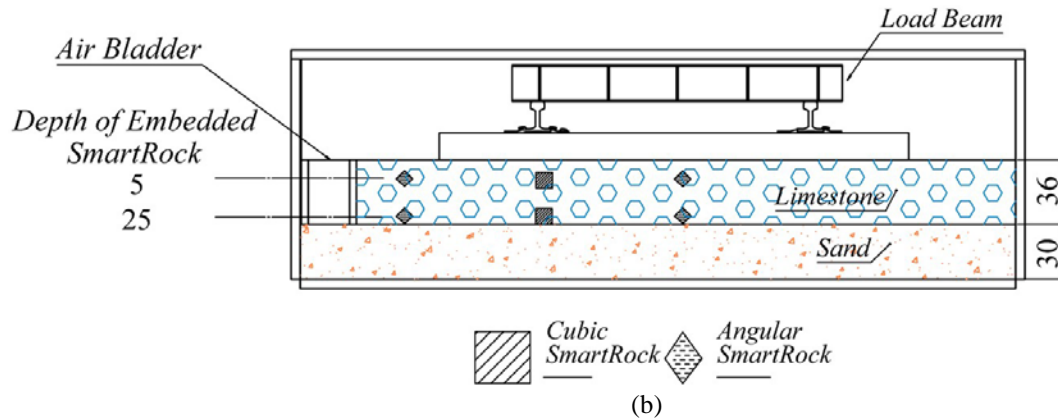
were used as the main equipment in the laboratory study (Figure 10). The ballast box was intended for loading the ballast in a controlled environment and to measure the ballast movement by using SmartRocks. A full-scale railway track structure, consisting of a ballast layer (36 cm thick), a sub-grade layer (30 cm thick), four concrete rail ties, two rails, and two I-beams, was constructed in the ballast box (Figure 11).



Figure 10 Photo of ballast box and loading system



(a)



**Figure 11 Geometry of track structure and location of SmartRocks in ballast box: (a) top view; (b) side view of test setup (all unit in cm)**



**Figure 12 Photo showing compacted subgrade and air bladders.**

Figure 11 shows where eight SmartRocks were embedded. The two cubic SmartRocks were embedded 5 cm and 25 cm under the rail seat of Tie 2 and two angular SmartRocks were embedded under the middle of Tie 2 at the same depths. The remaining four angular SmartRocks were embedded at 5 cm and 25 cm beneath the tie end and between Tie 2 and Tie 3. During construction, both the subgrade and ballast aggregates were placed into the ballast box in three equal-thickness layers (i.e., 12 cm thickness for each ballast layer and 10 cm thickness for each subgrade layer) and compacted.

Two air bladders of 152 cm (long)  $\times$  30 cm (wide)  $\times$  20 cm (high) with a capacity of 200 kPa (30 psi) were designed and embedded on one side of the ballast layer (Figure 12). In the ballast box tests, the air bladders were first fully inflated to simulate the confined shoulder condition, and subsequently deflated to simulate the lateral removal of shoulder.

Harmonic loading was applied through a reconfigurable loading frame on two I-beams crossing the rails (Figure 13). Two actuators with a load capacity of 490 kN (110 kips) each were utilized to conduct the tests. The magnitude of the load and the way it is applied to the ties are critical factors

affecting ballast performance and failure mode (Selig and Waters 1994). Based on field monitoring, Yin et al. (2017) suggested that the motion of a railroad crosstie under train loading could have both translational and rotational movements. In other words, ties not only push down but also knead the ballast while the train passes. To generate similar movements of the ties, the actuators were programmed to apply unsynchronized load to the two I-beams: the loads had the same magnitude but with a 180-degree phase lag between them. The magnitude and frequency of the loads were within the range of a typical train wheel (Huang 2010). In this study, tests were carried out in the load-controlled mode. A peak load of 160 kN (35.5 kips) and a peak load of 290 kN (65.5 kips) were used to represent a passenger train axle load and a freight train axle load, respectively. A total of 1,000 load cycles were applied for each test to enable investigation of ballast particle movement during different load and ballast conditions.

For each ballast, dry and wet conditions were tested. For the wet condition, water was introduced to the ballast layer from the top. The moisture contents of the clean and fouled ballast were 0.9% and 10.1%, respectively. The fouled ballast had a higher moisture content because finer grain aggregate holds more water. Table 1 presents the test matrix, including different combinations of ballast conditions (clean and fouled), moisture conditions (dry and wet), shoulder confinement, and loading conditions (magnitude and frequency).

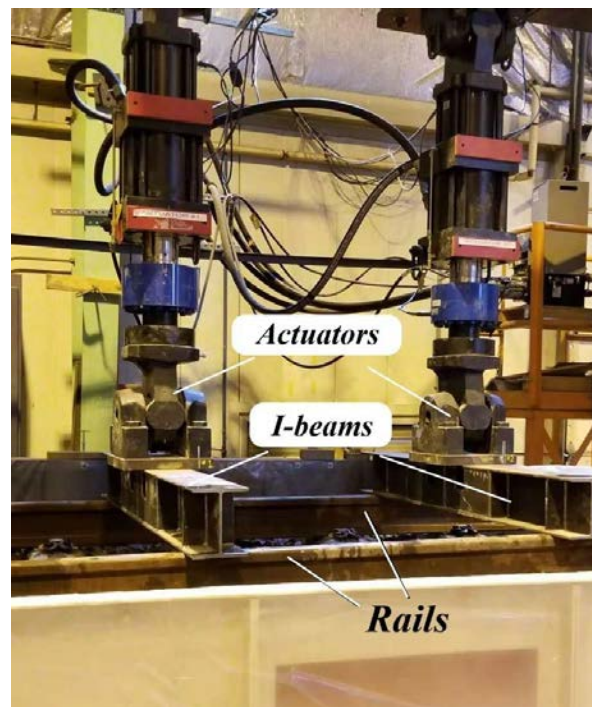


**Figure 13 Loading system**

**Table 1 Test Matrix for Ballast Box Test**

Test Group	Action Item #	Ballast condition	Moisture condition	Shoulder confinement	Load	Load frequency (Hz)
I	1	Clean	dry	Y	Passenger	1
	2	Clean	dry	Y	Freight	0.2, 1, 2
	3	Clean	0.9%	Y	Freight	1
	4	Clean	0.9%	N	Freight	1
II	1	Fouled	dry	Y	Passenger	1
	2	Fouled	dry	Y	Freight	0.2, 1, 2
	3	Fouled	10.1%	Y	Freight	1
	4	Fouled	10.1%	N	Freight	1

Track stiffness is the ratio between the line load and the track deflection. A reduction in track stiffness has a significant influence on the deterioration of the track (Frohling et al. 1996). In the tests conducted, the readings of LVDTs installed on the load actuators were utilized to calculate the track stiffness under different test conditions. The effect of three variables, moisture content, clean/fouled ballast, shoulder confinement, on track stiffness were and presented in Table 2. When one variable was investigated, the other variables were maintained the same. For example, Ballast Conditions (1) and (2) compares the impact of moisture content for the clean ballast with shoulder confinement while ballast conditions (4) and (5) compares the impact of moisture content for the fouled ballast with shoulder confinement; and Ballast Conditions (2) and (3) compares the impact of shoulder confinement for the clean-wet ballast.

**Table 2 Track Stiffness under Different Ballast Conditions**

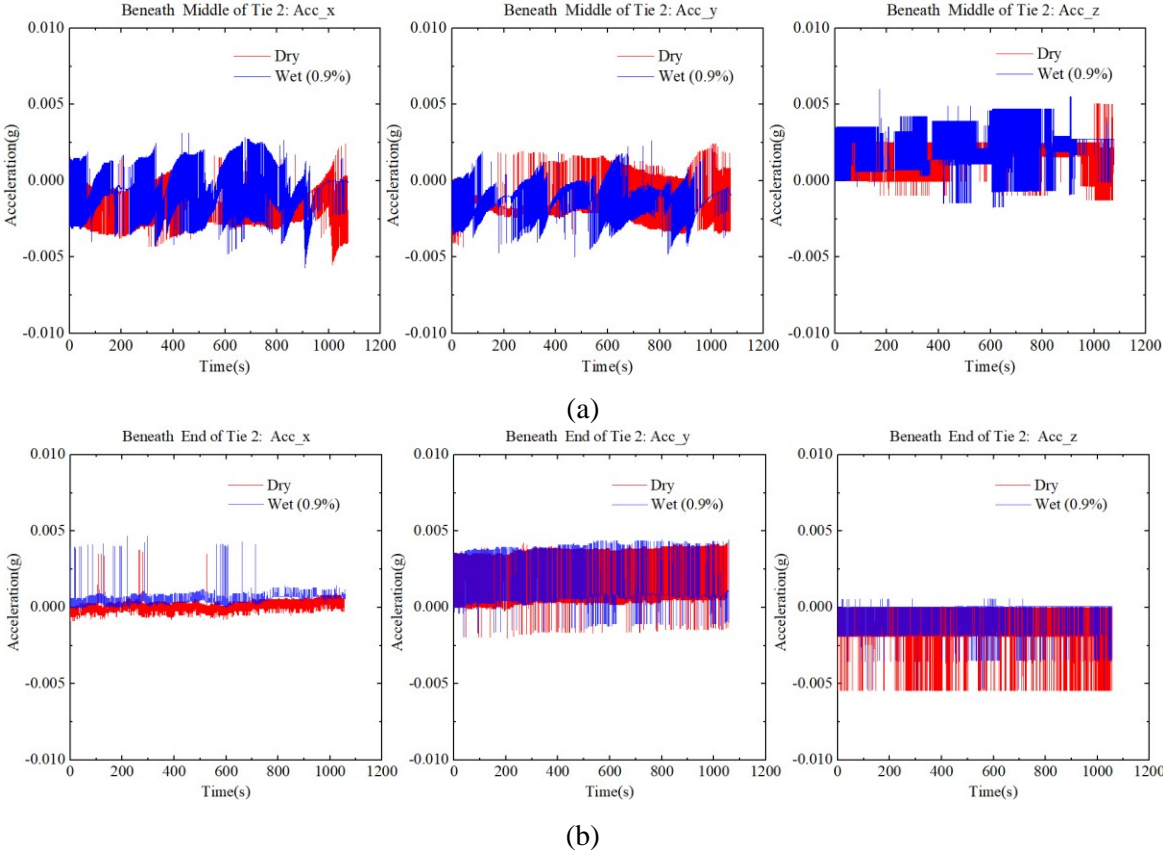
Ballast Conditions	(1). Clean, Dry, w/o Shoulder Removal	(2). Clean, Wet, w/o Shoulder Removal	(3). Clean, Wet, w/ Shoulder Removal	(4). Fouled, Dry, w/o Shoulder Removal	(5). Fouled, Wet, w/o Shoulder Removal
Track Stiffness (kN/mm)	29.65	29.31	27.41	21.79	19.18

Table 2 shows that track supported by fouled ballast, whether wet or dry, has a lower track stiffness value than track supported by clean ballast. It is also interesting to note that the track stiffness of track with fouled ballast is more sensitive to moisture conditions than track with clean ballast. A reduction in the track stiffness from 29.31 kN/mm to 27.41 kN/mm, when the shoulder was removed, shows a certain extent of rail track deterioration. Table 2 shows that a lower track stiffness can be resulted from fouled ballast and/or instable shoulder confinement that reduces support for track

loading.

SmartRock Results

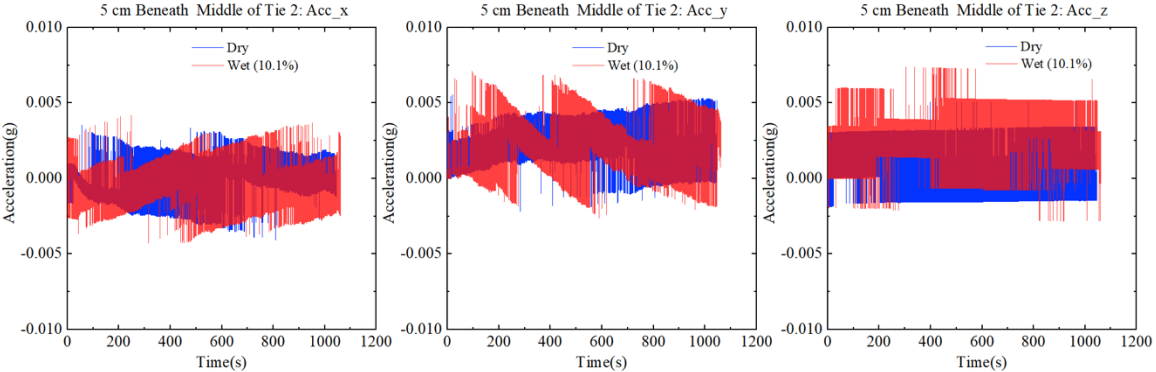
Since the track stiffness varies during the tests under different ballast conditions, ballast particles may experience different motions during cyclic loading. Translational accelerations and angular rotations were recorded by the SmartRocks and transmitted to a computer in real-time via Bluetooth. Figure 14 shows the recorded translational accelerations of the top SmartRocks (angular) 5 cm beneath the middle and end of Tie 2 in clean ballast under dry versus wet conditions. Figure 14 shows that for clean ballast, there is no apparent difference in the magnitude of particle accelerations especially the peak accelerations of the SmartRocks under dry and wet conditions at the two locations. This phenomenon was also observed in a field testing conducted by Huang et al. (2018). This is because water can drain rapidly from clean ballast and hence has little influence on particle movement.



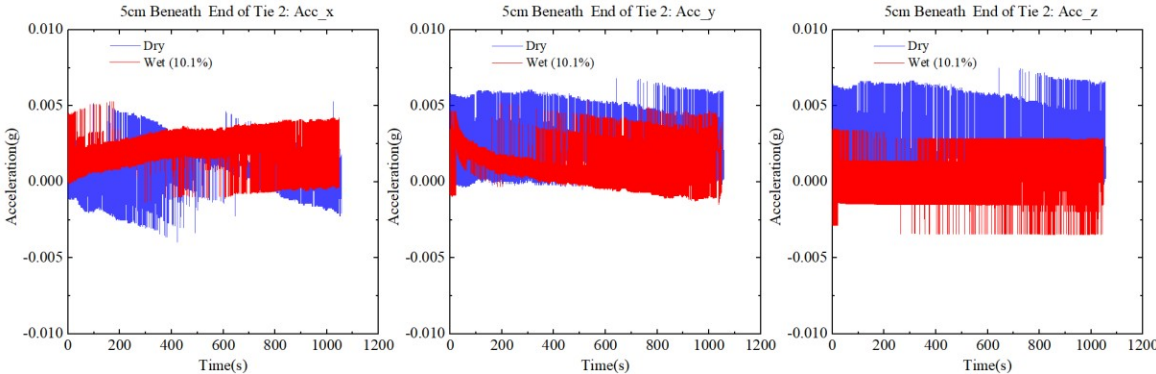
**Figure 14 Particle translational accelerations in clean ballast under dry versus wet conditions for top SmartRock beneath Tie 2: (a) middle of tie; (b) end of tie (1 Hz).**

Figure 15 shows the recorded translational accelerations of SmartRocks (angular) (both 5 cm and 25 cm) beneath both the middle and end of Tie 2 in fouled ballast under dry versus wet conditions. A comparison between Figure 14 and Figure 15 shows that the ballast particle movement in fouled ballast is more sensitive to moisture conditions. Figure 15 shows that the SmartRocks generally experienced higher translational accelerations with more fluctuation in the wet condition than in the

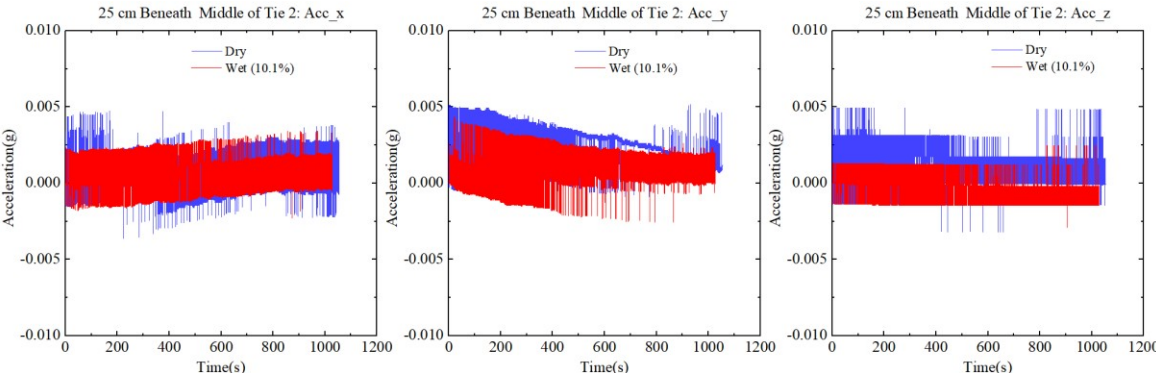
dry condition regardless of the location. This phenomenon can be explained because the intrusion of fine particles in fouled ballast reduces the drainage capacity of the ballast. Water held inside the ballast would serve as a lubricant causing a reduction in internal friction and, hence, facilitating movement of the ballast particles (Huang et al. 2009). The higher fluctuation of particle movement could also be attributed to higher dynamic pore water pressures in fouled ballast under wet conditions.



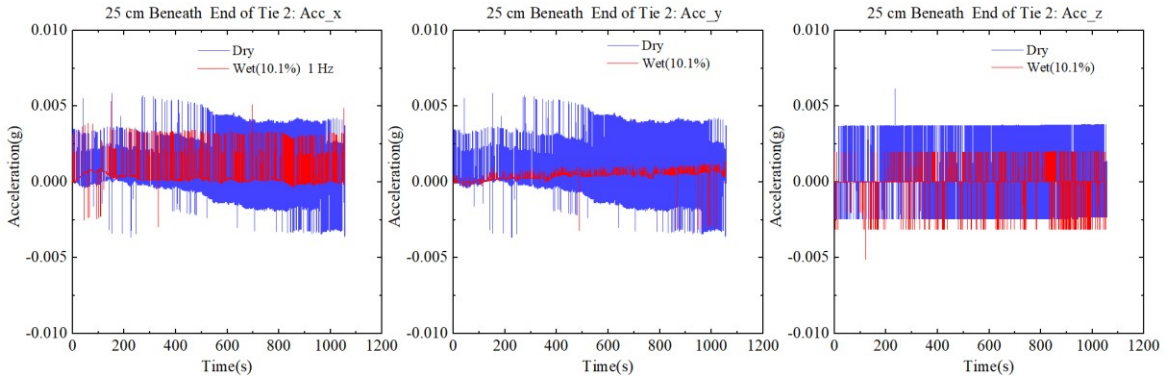
(a)



(b)



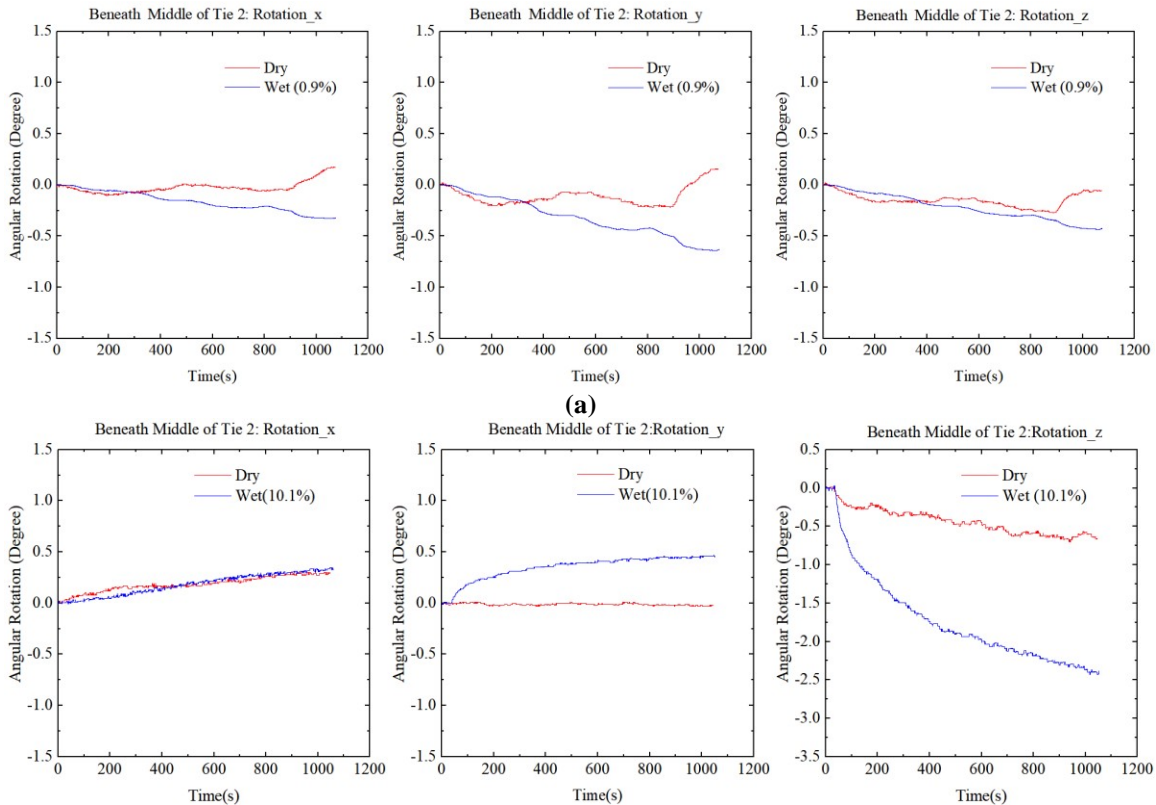
(c)



(d)

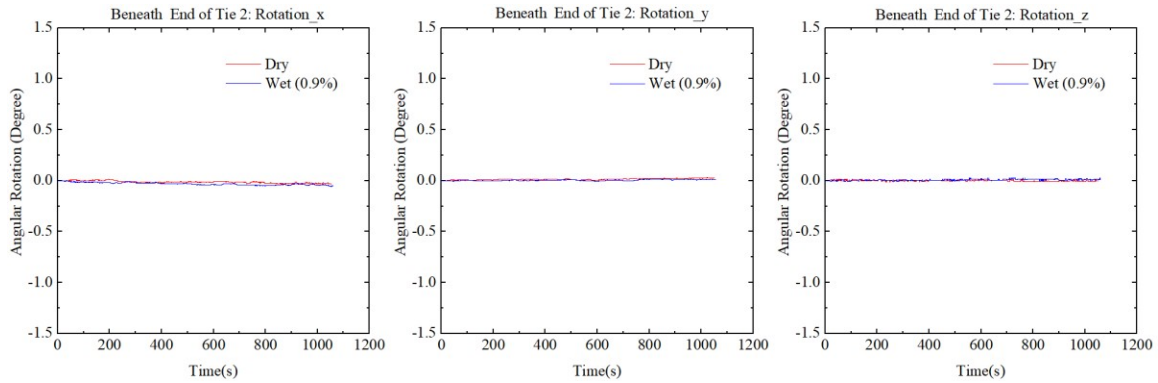
**Figure 15 Particle translational accelerations in fouled ballast under dry versus wet conditions for SmartRock beneath Tie 2: (a) 5 cm beneath middle of tie; (b) 5 cm beneath end of tie; (c) 25 cm beneath middle of tie; (d) 25 cm beneath end of tie (1 Hz).**

Similar effect of moisture content on angular rotations of the embedded SmartRocks is shown in Figure 16. A comparison between Figure 16 (a) versus Figure 16 (b) and Figure 16 (c) versus Figure 16 (d) shows that moisture content generally plays a more significant role on the rotational movement of ballast particles in fouled ballast than in clean ballast. For example, Figures 16 (a) and 16 (c) show that in the clean ballast condition, there is little apparent difference between the angular rotations under dry and wet conditions, particularly for the particles beneath the end of tie (see Figure 16 (c)). However, in the fouled ballast condition in Figures 16 (b) and (d), the angular rotations in wet condition are much higher than in dry condition.

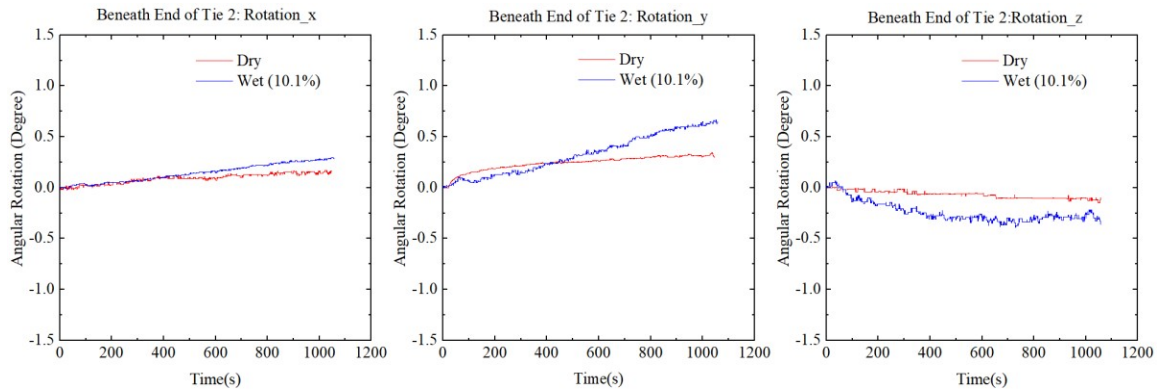


(a)

(b)



(c)



(d)

**Figure 16 Particle angular rotations of top SmartRock under dry versus wet conditions beneath Tie 2: (a) middle of tie: clean ballast; (b) middle of tie: fouled ballast; (c) end of tie: clean ballast; (d) end of tie: fouled ballast.**

### Summary

Ballast track performance and safety are largely dependent on ballast service conditions. Unfavorable ballast conditions (or “ballast defects”) will cause track geometry roughness and can contribute to increased rates of damage and deterioration to the rail, tie and fastening components. Ballast defects, if untreated, will eventually lead to ballast failure. Although ballast defects are often apparent through indications of poor geometry and structural degradation, maintenance and repair should be taken before the track displays noticeable deterioration in geometry. This research aims to develop and test a “Ballast Real-time Information System (BRIS)” that is able to detect “non-visual” ballast defects in an early stage and predict the possibility of future ballast in-service failure. SmartRock, as a core device in BRIS, has been instrumented in the ballast layer in the field and ballast box in the laboratory test. Based on the study, the following summaries are made:

- The easy and successful field deployment of the instrumentation shows its advantage at remote sites. SmartRocks are confirmed to be capable of recording particle movements under different ballast, loading, and moisture conditions; and may serve as a potential monitoring tool to monitor the ballast behavior and performance.

- The magnitude of ballast particle movement depends on track conditions: a track with mud pumping is likely have greater ballast particle movement.
- The influence of moisture content on particle movements in the clean and fouled ballast is different. The intrusion of fine particles in fouled ballast affects the drainage capacity of the ballast. The particle movements are much more sensitive to moisture content for the fouled ballast than the clean ballast.

## 5. Connect “SmartRock” network with cloud Discrete Element Modeling (DEM) computing to predict ballast performance

In this task, connections between “SmartRock” network has been set up and a computing scheme that is based on real-time data fusion between a sensing mechanism and real time (SMART) computing was developed, implemented and validated. This computing framework consists of: (1) real-time data acquisition of particle kinematics through a wireless instrumentation called “SmartRocks” that are embedded at discrete locations in a granular assembly, and (2) a built-in data-fusion-based algorithm using the Kalman filter to integrate the prediction generated by DEM and the measurements reported by “SmartRocks.” To evaluate the performance of the SMART computing algorithm, laboratory large-scale triaxial tests on ballast specimens were conducted and the results were compared to traditional DEM-only and SMART computing simulations.

### Sensing Mechanism and Real Time (SMART) Computing

The SMART computing framework consists of: (1) a real-time data acquisition device, SmartRock (hardware part); and (2) a built-in data- fusion-based algorithm for numerical simulations (software part). For the SMART computing, SmartRocks are first installed at discrete locations of interest during specimen preparation for measuring particle movements at these locations. DEM simulations are prepared in a traditional way except that those particles representing “SmartRocks” are positioned at the exact locations as those in the experiment. The SmartRock measurements are fused into the DEM simulation in real time through the built-in data-fusion-based algorithm.

This built-in data-fusion-based algorithm consists of two parts: The Kalman filter and DEM prediction. The Kalman filter is applied to recondition the calculated translations and rotations of the DEM particles which have the identical initial positions as the SmartRocks by learning from the SmartRock measurements. The DEM prediction is then applied to recondition the translations and rotations of the rest of DEM particles. The algorithm can be summarized as follows:

- (1) Compute state vector  $\begin{bmatrix} u \\ v \end{bmatrix}$  and  $\omega_k$  in DEM simulation at the  $k^{\text{th}}$  time step.
- (2) Import SmartRock measurements into DEM simulation.
- (3) Compute the difference between the SmartRock recordings and the DEM results for the particles corresponding to SmartRocks:

$$\Delta_k = MEAS_k - \begin{bmatrix} u \\ v \end{bmatrix}_k$$

$$\Delta_k = meas_k - \omega_k$$

- (4) Initialize the state covariance matrix:  $COV_0 = 0$ ,  $cov_0 = 0$ .  
(5) Update the state covariance matrix and compute the Kalman Gain matrix for particle translation:

$$COV_{k+1|k} = A \times COV_k \times A + Q_k$$

$$KG_{k+1} = \frac{COV_{k+1|k} \times H}{H \times (COV_{k+1|k} + R) \times H^T}$$

Update the state covariance matrix and compute the Kalman Gain matrix for particle rotation:

$$COV_{k+1|k} = cov_k \times q_k$$

$$kg_{k+1} = \frac{cov_{k+1|k} \times h}{h \times (cov_{k+1|k} + r) \times h^T}$$

where  $H$  and  $h$  are  $6 \times 6$  and  $3 \times 3$  identity matrices, respectively.  $KG$  and  $kg$  are the Kalman gains for particle translation and rotation, respectively. The Kalman gain is a relative weight given to the measurements and current DEM prediction. With a higher Kalman gain, more weight is placed on the most recent SmartRock measurements; whereas with a lower Kalman gain, more weight is given to the DEM predictions. If the Kalman gain equals to 1, the SmartRock measurements are 100% trusted; on the other hand, if the Kalman gain equals to 0, the DEM predictions are maintained.

$COV_{k+1|k}$  and  $cov_{k+1|k}$  are the prediction state covariance matrices based on the current state;  $COV_k$  and  $cov_k$  are the results of current state covariance matrices with respect to particle translation and rotation.  $R$  and  $r$  are the estimated covariance matrices of the noise from the SmartRock measurements.

- (6) Update the state vector and state covariance matrix of particle translation for the next iteration:

$$\begin{bmatrix} u \\ v \end{bmatrix} = \begin{bmatrix} u \\ v \end{bmatrix} + KG_{k+1} \times \Delta k$$

$$COV_{k+1} = COV_{k+1|k} - KG_{k+1} \times H \times COV_{k+1|k}$$

- (7) Complete DEM predictions.

In the experiments and simulations of a granular assembly, the ideal scenario would be the situation that all particles involved are SmartRocks so that movement of all particles can be monitored, subsequently fused into DEM using the Kalman filter algorithm. In most cases, however, only a limited number of particles can be replaced by SmartRocks due to practical reasons (e.g., cost) and computational expense. In other words, not all DEM particles have accurate descriptions from the SmartRocks. Hence, SmartRocks are strategically placed inside the granular assembly to form a series of “control nodes.” Contact forces of regular particles or “non-SmartRock” particles in the

DEM simulation are updated based on their contacts with these control nodes through the contact model.

#### (8) Model stability consideration.

In numerical simulations, a numerical model is stable if: (a) there is limited oscillation in the solution such that the numerical error does not build up whereby the solution stays close to the truth; and (b) it guarantees a bounded solution irrespective of timestep size [39]. A discussion on the stability limits of the most commonly used time integration schemes for discrete mechanical systems is provided by Rougier et al. In order to limit system oscillation, the particle kinematic behavior is iteratively performed for all contact points until the system reaches an equilibrium state using the following convergence criterion:

$$aratio \leq \delta$$

and to provide a basis for comparing the performance of DEM-only and the SMART computing simulations. The following sections describe the laboratory test first, then descriptions are given on how the numerical simulation model was prepared. Both the DEM-only and SMART computing simulations were prepared in the same way with the same parameters except that the particles considered as “control nodes” in the SMART computing were able to communicate with the associated SmartRocks and integrate the SmartRock measurements into the simulations. In the end, the results from the DEM-only and SMART computing simulations were compared with the laboratory tests.

#### Triaxial tests and simulations

In order to validate the proposed algorithm discussed above, a series of triaxial shearing tests were conducted under three confining pressures of 55 kPa, 110 kPa and 165 kPa to generate experimental results, and to provide a basis for comparing the performance of DEM-only and the SMART computing simulations. The following sections describe the laboratory test first, then descriptions are given on how the numerical simulation model was prepared. Both the DEM-only and SMART computing simulations were prepared in the same way with the same parameters except that the particles considered as “control nodes” in the SMART computing were able to communicate with the associated SmartRocks and integrate the SmartRock measurements into the simulations. In the end, the results from the DEM-only and SMART computing simulations were compared with the laboratory tests.

#### Laboratory tests

A series of large-scale triaxial tests were performed using a ballast triaxial tester. The test specimen dimensions are 30.5 cm in diameter and 61.0 cm in height. The acrylic chamber of the testing device has dimensions of 61.0 cm in diameter and 122.0 cm in height. A load actuator with a capacity of 89 kN is placed on top of the specimen top platen. Figure 17(a) shows a photo of a ballast specimen assembled inside the acrylic chamber ready to be transported to the loading frame. The ballast material used in the tests was a clean granite with 100% crushed aggregates. The properties met the American Railway Engineering and Maintenance-of-Way Association (AREMA) No. 4 gradation

specification.

A total of ten SmartRocks were numbered and placed in the specimen at different locations, as shown in Figure 17(b). Four SmartRocks were placed at the interface between the second lift and the third lift, as well as between the third lift and the fourth lift, one at the center and the other three evenly distributed along the circumference next to the membrane. Two SmartRocks were placed at the interface between the first and the second lift, one at the center and the other one next to the membrane. All the SmartRocks placed next to the membrane were vertically aligned with the corresponding SmartRocks in the adjacent layer(s). Before each test, the position of each SmartRock was recorded, and its orientation was read from the SmartRock measurements. This information was used to guide the generation of SmartRock particles in DEM simulations to be discussed later.

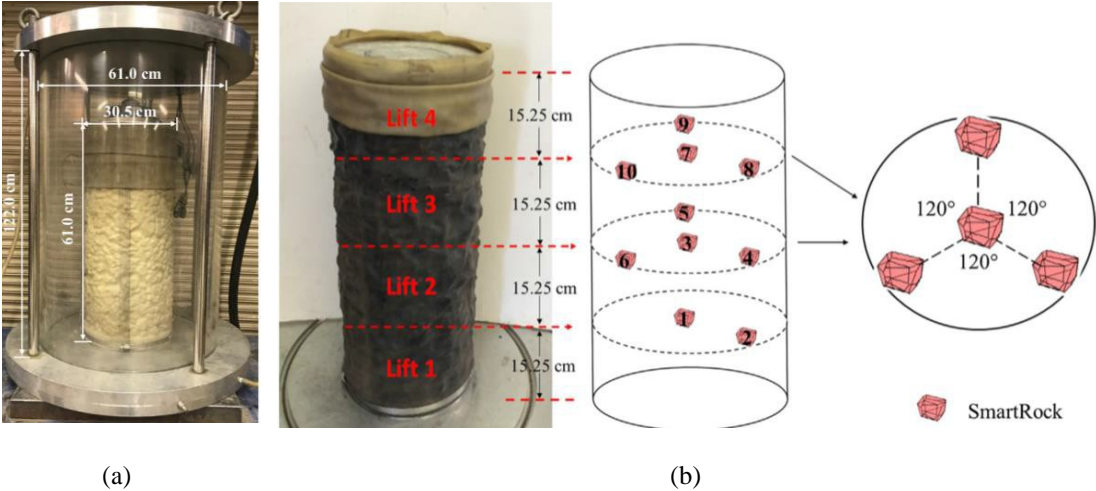


Figure 17 SmartRocks in specimen.

A displacement control mode at a slow shearing rate of 0.5% axial strain per minute, corresponding to 0.051 mm/s with a 61-cm high ballast specimen, was chosen for the test. The shearing rate was relatively slow so that: (1) the test could have more tolerance for specimen misalignment and less safety concern in the laboratory environment; (2) the operator could better control the test boundary conditions; and (3) more movement data could be recorded by the SmartRocks during the shear test.

Numerical simulation

- Model preparation

For simulating a laboratory triaxial test, it is necessary to model the flexible membrane behavior (i.e., specimen latex membrane). A total of 96 rigid rectangular wall elements (in eight layers) were used to form a cylindrical membrane chamber. Each layer had twelve equal-sized elements and each element was 20.32 cm long, 10.16 cm wide, and 7.62 cm high. These elements were only allowed to move in the radial direction. The movements in the other directions were restricted to replicate the deformation of the membrane. And in order to create a ballast specimen in the DEM model, the SmartRocks were first generated. These generated SmartRocks had the same position and orientation as those in the laboratory test (see Figure 17(b)). A library of ten DEM particle clumps was generated

by connecting thirty spherical balls together to mimic shape characteristics of ballast particles (i.e., AI and F&E ratio). The generated clumps were then poured into the cylinder. The generated SmartRocks were fixed temporarily until the generation of ballast specimen was completed. By selecting an appropriate height to let particles fall down under gravity, the specimen was allowed to reach an equilibrium state with a porosity close to the target value of 0.32. Figure 18 compares the specimen generated by the polyhedral shaped ballast particles with the corresponding DEM clumps.

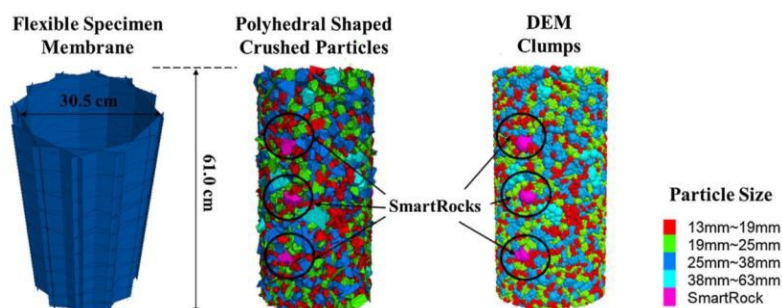


**Figure 18 Illustrations of triaxial ballast specimen in DEM simulations**

A consistent confining pressure was imposed on each layer of the wall in a “servo-control” fashion. The membrane simulated in this way functions as follows: (1) the bulging shape of the specimen can be possibly simulated as the radial movement of each layer can be varied conveniently with no friction exists between membrane elements; and (2) computation time can be greatly reduced as the confining pressure of each wall element can be simultaneously adjusted through multiple servo-control mechanisms. The shearing was performed by moving the top platen vertically. An approach based on the “Incremental Displacement Shearing Method (IDSM)” was adopted to simulate the shearing rate. The 8% total axial strain was reached after 800 incremental displacement stages. At each stage, the top platen moved by  $6.1 \times 10^{-4}$  mm, corresponding to 0.01% axial strain and then simulation was continued while the system was re-equilibrated before the next incremental displacement was applied.

Two types of numerical simulations were conducted in this study: the DEM-only and SMART computing simulations. Both simulations used the same packing assembly, model parameters, and loading conditions. The parameters, shown in Table 3, were calibrated through trial and error to match the stress-strain behavior of a laboratory test. The wall stiffness and clump stiffness were kept the same, while the particle friction coefficient was varied until the simulation results were comparable to the experimental results. After selecting the particle friction coefficient, the ratio of normal contact stiffness to shear contact stiffness of clump was varied to match the volumetric change. Third, the ratio of normal to shear contact stiffness of clump remained the same, the normal contact stiffness and shear contact stiffness of clump were adjusted proportionally until the simulation results had no significant change. In the end, the wall stiffness was varied to check its effect on the stress-strain behavior. It was found that the wall stiffness did not significantly change the stress-strain behavior of the specimen within the range of values considered; therefore, the smallest stiffness value was selected in order to conduct large scale simulations with a relatively larger time-step (i.e., time-step is inversely related to stiffness).

**Table 3 Model parameter used in ballast triaxial test DEM simulation**

DEM Model Parameter	Value
Clump Density	2750 kg/m <sup>3</sup>
Friction Coefficient	0.7
Wall normal stiffness	1 × 10 <sup>8</sup> N/m
Wall shear stiffness	1 × 10 <sup>8</sup> N/m
Clump normal stiffness	0.63 × 10 <sup>8</sup> N/m
Clump shear stiffness	0.63 × 10 <sup>8</sup> N/m
Damping	0.7

- Algorithm deployment

The SmartRock measurements were used to correct the kinematic status of the control nodes in PFC3D. The measurements were saved in a plain text file, which was subsequently imported to PFC3D and the measurement data are stored in a matrix using the Fish language. Particle positions were adjusted through the SMART computing at desired time intervals. Choosing an appropriate time interval to evoke the SMART computing algorithm warrants careful consideration. On one hand, the simulation requires a sufficient number of algorithm executions to yield accurate and reliable solutions because the more frequently the SMART computing is executed, the more accurate descriptions of particle kinematic information the system has. On the other hand, the computation efficiency needs to be considered. Therefore, a balance between the two criteria (accuracy and efficiency) needs to be achieved. Evoking the algorithm at an interval of every 0.01% axial strain increment was found to provide satisfactory results in this study and therefore used in all simulations.

During the SMART computing, the kinematic behavior of the control nodes was updated first; the updated control nodes interacted with the surrounding particles to update the behavior of the rest of particles. The equilibrium state was checked and re-achieved if needed after execution of the SMART computing.

### Results and discussions

Fig. 18 compares the deviatoric stress and volumetric strain vs. axial strain of the ballast specimen under the confining pressures of 55 kPa, 110 kPa and 165 kPa from the laboratory tests and the DEM-only and SMART computing (SC) simulations. The laboratory test results are generally consistent with the ballast behavior reported in the literature. For example, the maximum deviatoric stress increased and final volumetric strain decreased with an increase in confining pressure; the specimen experienced a significantly greater dilation under lower confining pressure (e.g., 55 kPa) than under higher confining pressure (e.g., 110kPa and 165kPa); and the specimen under high confining pressure (e.g., 165 kPa) experienced an initial contraction. Figure 19 shows that both of the DEM-only and SMART computing simulations generally agreed well with the experimental data, suggesting that

the calibrated DEM input parameters are generally appropriate. Comparisons of the simulations with the laboratory test results, the DEM-only simulations underestimated the deviatoric stress; a slightly lower Young's modulus appeared in the DEM-only simulations, particularly during the initial loading range. Additionally, the DEM-only simulations could not accurately predict the contraction behavior during the initial loading, especially under higher confining pressures, i.e., 110 kPa and 165 kPa. The dilation behavior of the ballast specimen was generally over predicted by the DEM-only simulations. These discrepancies may be attributed to detailed micromechanical behaviors (e.g., particle rearrangement and particle rotation) that could not be accurately captured in the DEM-only simulations. Furthermore, the difference between clumped particles using spherical balls in DEM and the angular ballast particles in reality may have affected both the deviatoric stress and volumetric strain.

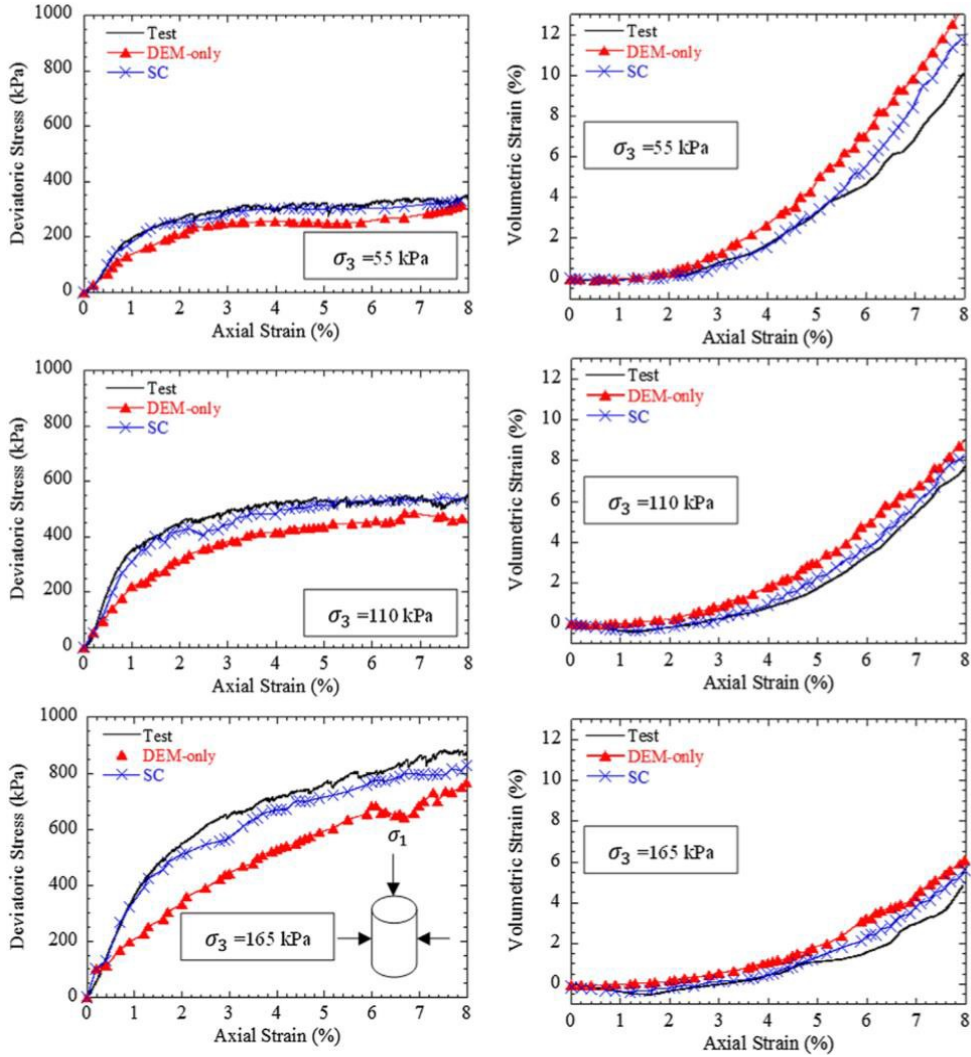
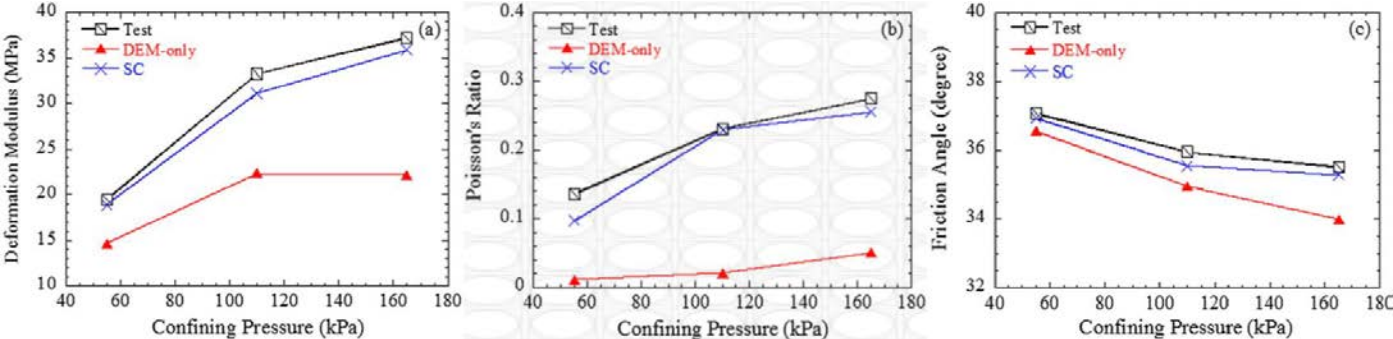


**Figure 19 Comparison of laboratory test, DEM-only, and SMART computing results: (a) deviatoric stress vs. axial strain; (b) volumetric strain vs. axial strain.**

In contrast, the deviatoric stresses and volumetric strains predicted by the SMART computing

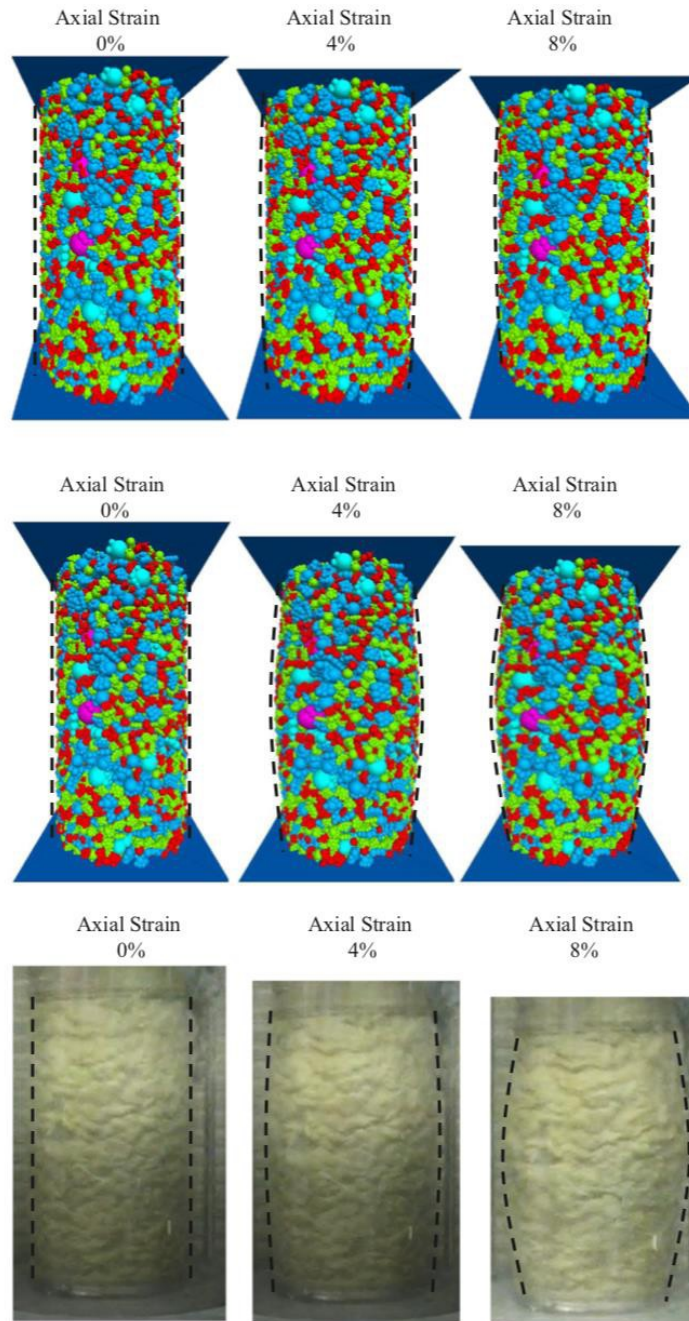
algorithm were much closer to the laboratory tests. In the SMART computing, the SmartRocks accurately recorded the actual movement through real-time translational and rotational measurements at first; when these measurements were incorporated into the DEM simulations, the SMART computing algorithm reconditioned the kinematic behavior of each control node where the SmartRocks were positioned by the Kalman filter algorithm; and the DEM simulation subsequently predicted the movement of the surrounding non-SmartRock particles based on the behavior of the control nodes. Once each particle in the ballast specimen had more accurate descriptions of the kinematic behavior, the stress and strain behavior of the specimen had better agreement with the laboratory test results at the macro level.

Figure 20 shows the macroscopic trends or properties of engineering behavior, e.g., deformation modulus, Poisson’s ratio, and mobilized friction angle under different confining pressures for the laboratory test, DEM-only, and SMART computing (SC) simulations. These properties were back calculated using the stress-strain behavior shown in Figure 19. The deformation modulus and the Poisson’s ratio increased as the confining pressure increased as shown in Figure 20(a) and (b), whereas the friction angle decreased as the confining pressure increased as shown in Figure 20(c). These trends are generally consistent with our understanding of the behavior of granular materials.



**Figure 20 Variations of macroscopic properties with confining pressure for the laboratory tests, and DEM-only and SMART computing predictions: (a) deformation modulus; (b) Poisson’s ratio; (c) friction angle.**

Comparing the material properties obtained from the two simulations, the results from the SMART computing were much closer to those from the laboratory tests. Figure 21 illustrates the deformed ballast specimen in the DEM-only (Figure 21(a)), SMART computing simulations (Figure 21(b)), and the laboratory test (Figure 21(c)) at 0%, 4%, and 8% axial strains under the confining pressure of 55 kPa. The laboratory test shows that the specimen had a significant bulging shape at the midsection of the specimen as the axial strain increased, indicating the ballast specimen was experiencing shear failure. In the DEM-only simulations, it can be seen that the radial dimension of the specimen increased almost evenly with the loading, without exhibiting the bulging shape. However, the evolution of the bulging shape was successfully captured using the SMART computing, and the simulated final configuration of the specimen had a good agreement with that in the laboratory test.



**Figure 21 Deformed ballast specimen configuration at different loading stages under 55 kPa confining pressure:  
(a) DEM-only; (b) SMART computing; (c) photo from the laboratory test.**

To provide a more quantitative comparison of the deformed shape of the specimen, Figure 22 compares the radial deformations measured in the test, DEM-only, and SMART computing (SC) simulations at the axial strain of 8%. In figure 22, each curve represents an approximation of the overall deformed shape. The radial deformation at the center of each layer was used to evaluate the deformed shape. The deformed geometry from the test shows a bulging shape of the specimen that

greater radial deformation occurred in the middle of the specimen. In the DEM-only simulations, the specimen evenly deformed and the bulging shape was not evident. The SMART computing was able to simulate the bulging shape successfully, and the deformed geometry had a better agreement with the specimen final configuration from the test results.

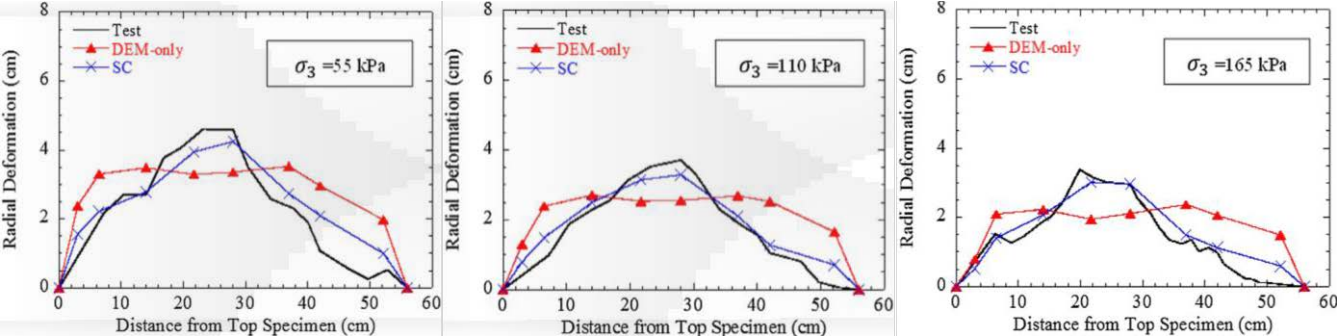


**Figure 22 Radial deformations of specimens from the laboratory test, and DEM- only and SMART computing simulations at 8% axial strain.**

Summary

In this task, it presents a SMART computing algorithm that can enhance DEM simulations using a wireless device - “SmartRock.” The SmartRock is capable of recording real-time particle translation and rotation if embedded in a granular assembly. The SMART computing is a Kalman-filter-based data fusion technique that can incorporate real-time SmartRock recordings into DEM simulations to improve the accuracy of the latter. In the simulation, only a small percentage of particles are replaced by SmartRocks to have accurate kinematic descriptions while movements of the other non-SmartRock particles, i.e., most aggregates in the tested specimens in this study, are accurately predicted using this algorithm.

Simulation results, including deviatoric stress, volumetric strain, deformation modulus, and vertical and radial deformation, using the DEM-only and SMART computing were compared with the laboratory triaxial test results. The radial deformation of the specimen upon shearing was successfully captured by the SMART computing. The laboratory specimen bulging effect was also predicted accurately in the SMART computing simulations. In general, the simulated stress-strain behavior using the SMART computing had better agreement with the laboratory tests than the DEM-only simulations did.

The SMART computing is considered as an effective algorithm to precondition the particle movement at an individual particle level, and hence to improve the accuracy at a macro level. This study indicates that the SMART computing, if implemented with appropriate physical models, can be used to simulate the large scale shearing tests with high fidelity and accuracy. The SMART computing algorithm can be coupled with other numerical methods, such as the finite element method and the smoothed particle hydrodynamics method, to solve a wide range of challenging civil engineering problems. With the development of smaller sensing and data transmitting technologies, the SMART computing algorithm will expand its applications beyond civil engineering.

## Conclusions

In this project, a wireless device – “SmartRock” was designed and manufactured to monitor the rail ballast particle movement under different ballast conditions. Both the laboratory test and field test have been conducted with the applications of SmartRock. Finally, a numerical scheme that is based on real-time data fusion between a sensing mechanism and real time (SMART) computing was developed, implemented and validated. From all the tasks, conclusions have been made as following:

(1). The SmartRock is capable of recording real-time particle translation and rotation under different ballast, loading, and moisture conditions if embedded in a granular assembly. SmartRock can serve as a potential monitoring tool to monitor the ballast behavior and performance in the field.

(2). A pattern recognition technique (this component is in our paper under review and is omitted in this report due to page limitation) - Autoregressive (AR) model with X-bar control chart - was used to differentiate ballast conditions based on particle movements has been set up and validated in the laboratory environment and ready for field deployment. It can be used to identify changes in particle movement patterns under different conditions. Using the clean ballast performance as the baseline, the AR model is capable of identifying ballast fouling and shoulder instability. A threshold value of 20% for the percentage of outliers of ballast particle movement patterns is suggested for the test conditions considered in this study. Additional field studies are needed to identify the range of threshold values for a broad range of field conditions, including ballast material, train loading, moisture content, and lateral confinement.

(3). The Sensing Mechanism and Real Time (SMART) computing has been proven to be an effective algorithm to predict granular material behavior. The combination of SmartRock sensor network, Pattern Recognition technique and the SMART Computing technology is promising in terms of accurate ballast performance monitoring.